BioMol Concepts, Vol. 2 (2011), pp. 53–64 • Copyright © by Walter de Gruyter • Berlin • New York. DOI 10.1515/BMC.2011.005

Review

Solution NMR studies of periplasmic binding proteins and their interaction partners

Sara Pistolesi[1], Nico Tjandra[1] and Guillermo A. Bermejo[2,*]

[1] Laboratory of Molecular Biophysics, National Heart, Lung, and Blood Institute, National Institutes of Health, Bethesda, MD 20892, USA
[2] Division of Computational Bioscience, Center for Information Technology, National Institutes of Health, Bethesda, MD 20892, USA

*Corresponding author
e-mail: bermejog@mail.nih.gov

Abstract

Periplasmic binding proteins (PBPs) are a crucial part of ATP-binding cassette import systems in Gram-negative bacteria. Central to their function is the ability to undergo a large-scale conformational rearrangement from open-unliganded to closed-liganded, which signals the presence of substrate and starts its translocation. Over the years, PBPs have been extensively studied not only owing to their essential role in nutrient uptake but also because they serve as excellent models for both practical applications (e.g., biosensor technology) and basic research (e.g., allosteric mechanisms). Although much of our knowledge at atomic level has been inferred from the detailed, static pictures afforded by crystallographic studies, nuclear magnetic resonance (NMR) has been able to fill certain gaps in such body of work, particularly with regard to dynamic processes. Here, we review NMR studies on PBPs, and their unique insights on conformation, dynamics, energetics, substrate binding, and interactions with related transport proteins. Based on the analysis of recent paramagnetic NMR results, as well as crystallographic and functional observations, we propose a mechanism that could explain the ability of certain PBPs to achieve a closed conformation in absence of ligand while others seem to remain open until ligand-mediated closure.

Keywords: ABC transporters; glutamine-binding protein; maltose-binding protein; nuclear magnetic resonance; paramagnetic relaxation enhancement; periplasmic binding proteins.

Introduction

ATP-binding cassette (ABC) transport systems constitute one of the largest protein superfamilies. They couple ATP hydrolysis to the translocation of substrates across cellular membranes, and are involved in an overwhelming variety of biological processes, ranging from bacterial nutrient uptake to human diseases (1). ABC transporters share a common organization: two multi-span transmembrane domains associated with two cytosolic ATP-binding domains (the ABCs). In the case of importers, most additionally rely on a high-affinity binding protein that acts as a primary receptor, essential for capturing a specific substrate molecule and presenting it to the membrane-associated machinery for translocation. Gram-negative bacteria display such binding proteins as soluble polypeptides in the periplasmic space, earning them the generic name of periplasmic binding proteins (PBPs).

A PBP is a single-chain polypeptide with a mass in the 25–60 kDa range, and can bind one or more ligand types with high affinity (0.01–1 μM). Thus, for instance, whereas maltose-binding protein (MBP) binds a series of maltooligosaccharides, glutamine-binding protein (GlnBP) binds L-glutamine with high specificity. Collectively, however, PBPs handle a wide variety of ligands, ranging from peptides to inorganic ions. The central role of PBPs in the nutrient uptake process is highlighted by the fact that the ATP-dependent translocation across the membrane is initiated by the conformational change that accompanies ligand binding, and not the substrate directly.

Knowledge on how PBPs function has been deeply enhanced by the availability of three-dimensional structures of numerous members of this large family. Such structures primarily stem from X-ray crystallography studies, which have been extensively reviewed both exclusively in terms of PBPs (2–7) and in the larger context of complete ABC importer systems (8–14). Here, we review structural PBP research conducted in aqueous solution, where nuclear magnetic resonance (NMR) spectroscopy has shed unique light on molecular structure and dynamics, conformational energetics, binding affinity, binding mechanism, and protein-protein interactions.

Are X-ray structures crystal clear?

Although the PBP family displays a range of sizes, diversity of substrates, and lack of high sequence similarity, crystal structures reveal a common architecture for all its members: two globular domains or lobes that share a similar size and topology, each comprising pleated β-sheets surrounded by α-helices. One or more polypeptide segments link the domains to each other; in the case where the number of segments is odd, the N- and C-terminus fall in different domains, and can be used to name the latter as in the N- and

C-domain of MBP (Figure 1). In the absence of substrate the two domains of a PBP are typically far from each other, separated by a deep solvent-accessible cleft or groove (Figure 1A). A dramatic conformational change transforms this 'open' configuration into a 'closed' one, exhibited by liganded structures, where the substrate occupies the cleft and the two domains come close to each other, making extensive contacts with the substrate which becomes highly sequestered from the surrounding solvent (Figure 1B). Because the structure of the individual domains remains largely unchanged in liganded and unliganded versions of a PBP, and only differences in their relative position and orientation are observed, the conformational transition can be regarded as a rigid-body-domain process where the linker segments function as a hinge.

In addition to the common open-unliganded and closed-liganded configurations, crystallographic studies have also yielded a few structures that are (i) closed-unliganded, as in glucose/galactose-binding protein (GGBP) (15) and choline-binding protein (ChoX) (16), and (ii) open-liganded, as in leucine/isoleucine/valine-binding protein (LIVBP) (17) and MBP (18–20). The open-liganded structures have been achieved by either soaking crystals of an open-unliganded form with a solution of natural substrate (17, 19) or cocrystallizing the PBP with an inactive ligand (18–20); in each case the ligand preferentially interacts with one of the two domains.

Given that the conformational change between a substrate-free and -bound PBP represents a crucial control mechanism for transport and signal transduction processes, the characterization of the tertiary structures of both protein forms has become an important research goal. In the crystal state, however, the relatively wide range of opening angles observed for different unliganded PBPs suggests that 'the extent of opening is likely to be influenced by crystal packing constraints' (7). Indeed, even the same PBP can yield various distinct unliganded structures upon crystallization, as in ribose-binding protein (RBP) (21), allose-binding protein (22) and its mutant engineered to bind serotonin (23), LIVBP (24), ChoX (16, 25), leucine-binding protein (26, 27), and GGBP (15, 28). Closed-liganded conformations – where the two domains are stabilized by multiple interactions with the sandwiched ligand – are less likely to suffer from such strong crystal lattice effects. Furthermore, the latter are not expected to occur for all unliganded PBPs, as confirmed by solution NMR on MBP (29) and GlnBP (30), and solution small-angle X-ray scattering (SAXS) on a MBP mutant (31) (see below). Nevertheless, the interdomain angle variability in the above crystallographic examples highlights the need for studies aimed at establishing the average structure in solution.

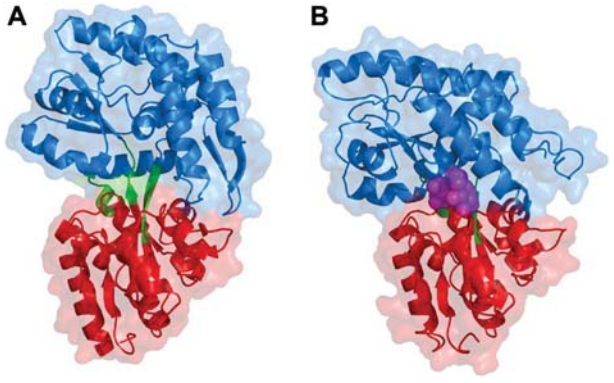

Figure 1 Crystallographic models of maltose-binding protein (MBP), a representative PBP. The N-domain is colored red, the C-domain blue, and the linker segments green; backbone traces are shown along with the translucent surface representation of all heavy atoms. The open-unliganded conformation (PDB ID 1OMP) is displayed in (A), and the closed, maltotriose-loaded (PDB ID 3MBP) in (B). Maltotriose atoms are displayed as magenta spheres. N-domain backbone atoms were used to align both structures prior to their lateral translation into (A) and (B). All graphical representations of atomic coordinates were generated with PyMOL (http://pymol.org).

Despite that the solution structure of a PBP can be determined *de novo* by NMR, as demonstrated with MBP (32), a significantly more straightforward strategy, when a crystal form of the protein is available, consists of realizing that the conformation of the individual domains is less likely to be affected by crystal packing than that of the hinge region. This assumption, along with the known rigid-body-domain behavior mentioned above, transforms the NMR solution structure elucidation problem into one of finding the relative three-dimensional arrangement of the two domains, whose individual structures are those previously determined by X-ray crystallography. The outcome of this hybrid approach is henceforth referred to as the 'solution structure' of a PBP, making the necessary exception when alluding to the above-noted sole *de novo* model (32).

Starting from an available X-ray structure of a PBP in a given conformation, the interdomain configuration in solution can be found by maximizing the agreement of certain interatomic bond orientations (e.g., peptide backbone N-H) with those experimentally inferred from residual dipolar couplings (RDCs) [technique reviewed in Ref. (33)]. A salient example of this approach is the study of ligand-induced effects on the structure of wild-type MBP (29, 34) (structures of MBP hinge mutants are discussed in the following section). Whereas solution structures of MBP both unliganded and maltotriose-bound were found consistent with their crystal counterparts (29), that in complex with β-cyclodextrin revealed significant discrepancies (29, 34). The X-ray structure of MBP bound to β-cyclodextrin displays a fully open structure (i.e., virtually identical to unliganded MBP) (20), whereas the average conformation in solution is 11° more closed, although still more open than the maltotriose-bound structure which is 35° away from fully open. This result, based on the above-described hybrid X-ray/NMR approach, is consistent with the *de novo* NMR structure of β-cyclodextrin-loaded MBP (32) and with NMR relaxation experiments aimed at characterizing the rotational diffusion of the protein in solution (35). An NMR methodological review on this system can be found elsewhere (36).

The ability to accurately and straightforwardly determine average interdomain conformations in solution, as exempli-

fied by the above NMR studies, has proven to be crucial for the characterization of the energetic cost of PBP domain rearrangement and its relationship to ligand binding affinity.

Energetics of domain reorientation and binding affinity

Traditional studies on the ligand binding affinity of PBPs, as well as other proteins, have focused on the careful dissection of the different ligand-protein interactions at the binding pocket (2, 3, 5, 7). More recently, however, emphasis has been placed on residues that do not contact the ligand, located in the hinge region. Such efforts primarily stem from protein engineering initiatives [reviewed in Refs. (37, 38)], with the goal of increasing binding affinity by performing modifications far removed from the binding site instead of directly in it, as the latter approach often requires the delicate maintenance of stereochemical complementarity. Indeed, from the thermodynamic linkage relationships shown in Figure 2 it follows that the apparent binding affinity (given by $\Delta G^{App}_{Binding}$) can be enhanced not only by strengthening ligand-PBP contacts at the binding site (i.e., decreasing $\Delta G^{Closed}_{Binding}$) but also by destabilizing the ligand-free open conformation relative to the closed one (i.e., decreasing $\Delta G^{Free}_{Open\rightarrow Closed}$), because

$$\Delta G^{App}_{Binding}=\Delta G^{Free}_{Open\rightarrow Closed}+\Delta G^{Closed}_{Binding}. \quad (1)$$

The latter strategy has been demonstrated with MBP (31, 39) and relies on the existence of an interface in the hinge region, opposite the binding pocket, that becomes solvent-exposed upon interdomain closure (Figure 2). Perturbation

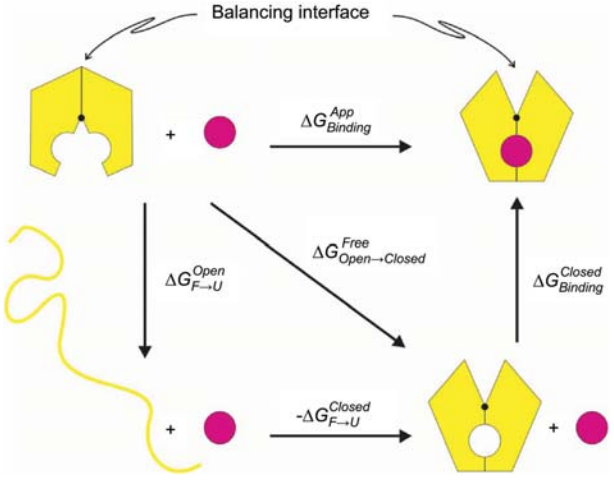

Figure 2 Thermodynamic linkage relationships involving MBP. The ligand is represented by a magenta circle. The protein is colored yellow and appears either in an unfolded state (line) or in a folded one (other). Folded protein displays either an open conformation (top left corner) or a closed one (right corners); the hinge is denoted by a black circle. The balancing interface and the nomenclature for the free-energy changes between thermodynamic states are indicated.

of stabilizing interactions across such so-called 'balancing interface' (31) disfavors the open conformation and concomitantly tightens binding. The disruption of the balancing interface can be achieved sterically by replacing one or more of its wild-type residues by bulkier ones. Thus, for instance, MBP I329W single mutant and I329W/A96W double mutant show 20- and 60-fold improvement in binding affinity relative to wild-type MBP, respectively (39).

An atomic level explanation of the above phenomenon has been afforded by a NMR study that determined the solution, unliganded conformations of a series of five MBP mutants (40) (I329X and the I329W/A96W double mutant; for the complete set, see Figure 3), following the RDC-based method discussed in the previous section. Such structures display different average interdomain closure angles around a common hinge axis, ranging from 5.5° (I329C) to 28.4° (I329W/A96W), and, along with the solution conformations of wild-type unliganded MBP (0° closed by definition) and maltotriose-MBP (35° closed) (29), they trace the trajectory between the fully open and fully closed states. Careful inspection of this set of structures reveals that the greater the degree of closure, the more non-polar surface area at the balancing interface is exposed to the aqueous environment (40). Furthermore, protein stability, as assessed by the free-energy change of unfolding $\Delta G^{Open}_{F\rightarrow U}$ (Figure 2) (excluding the contribution of the mutation, a correction assumed henceforth), decreases linearly with the closure angle at a rate of 212±16 cal/mol/deg (Figure 3) (40). This suggests the solvent exposure of non-polar residues at the balancing interface as the source of instability.

Figure 2 indicates that $\Delta G^{Free}_{Open\rightarrow Closed}$ and $\Delta G^{Open}_{F\rightarrow U}$ are related via

$$\Delta G^{Free}_{Open\rightarrow Closed}=\Delta G^{Open}_{F\rightarrow U}-\Delta G^{Closed}_{F\rightarrow U}, \quad (2)$$

where the newly introduced symbol $\Delta G^{Closed}_{F\rightarrow U}$ is the free-energy change of unfolding of the unliganded, closed conformation. Inserting Eq. (2) into Eq. (1) yields

$$\Delta G^{App}_{Binding}=\Delta G^{Open}_{F\rightarrow U}-\Delta G^{Closed}_{F\rightarrow U}+\Delta G^{Closed}_{Binding}. \quad (3)$$

Assuming the mutations do not affect the liganded conformation, as expected from their distal location to the binding site, $\Delta G^{Closed}_{F\rightarrow U}$ and $\Delta G^{Closed}_{Binding}$ are constant. Therefore, any mutation-induced interdomain closure angle dependence observed in protein stability ($\Delta G^{Open}_{F\rightarrow U}$) should be reflected in the binding affinity. Indeed, measurements of binding constants of wild-type MBP and its mutants for maltose produce a linear decrease of $\Delta G^{App}_{Binding}$ with increasing closure angle, at a rate of 151±38 cal/mol/deg (40), comparable to the rate obtained for $\Delta G^{Open}_{F\rightarrow U}$ (212±16 cal/mol/deg).

Increase in MBP binding affinity has been alternatively achieved by removal of favorable interactions at the balancing interface (e.g., loop deletion), which do not significantly affect the unliganded structure, as suggested by both crystallography and solution SAXS data (31). By contrast, the above-discussed bulky substitutions that modulate both affinity and interdomain closure angle have allowed a detailed

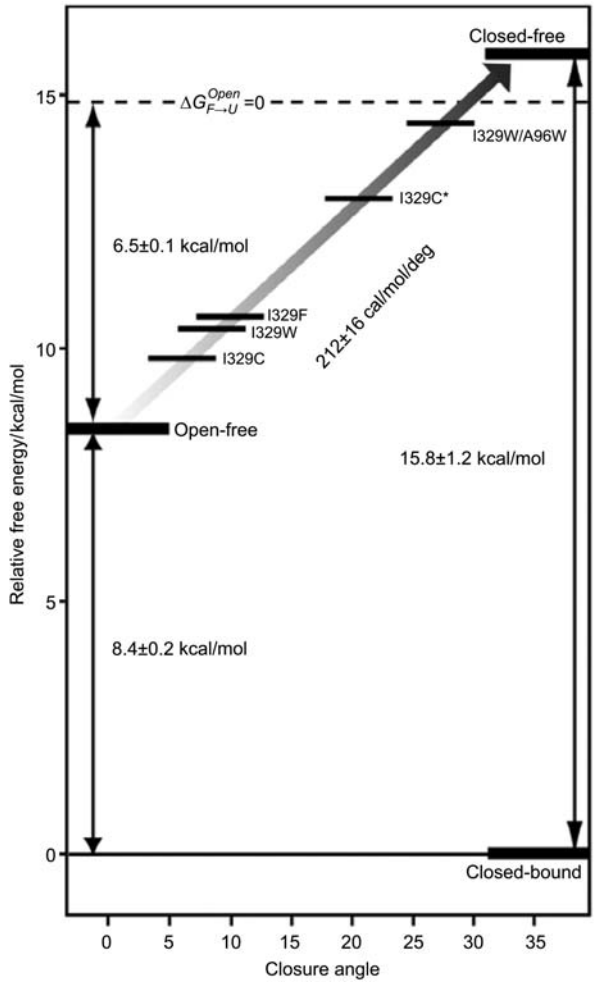

Figure 3 Dependence on interdomain closure angle of the relative free energy of a wild-type MBP polypeptide that adopts either the wild-type conformation or that of hinge mutants I329C, I329W, I329F, I329C*, and I329W/A96W (the asterisk indicates derivatization with *N*-((2-(iodoacetoxy)ethyl)-*N*-methyl)amino-7-nitrobenz-2-oxa-1,3-diazole). The closed-liganded state ('closed-bound') is arbitrarily set as the energy origin. The energy of a hypothetical closed-unliganded conformation ('closed-free') is calculated by extrapolation of the linear correlation extracted from the free-energy change of unfolding ($\Delta G^{Open}_{F\rightarrow U}$) for the unliganded MBP set, which has the wild-type conformation ('open-free') as the most stable member. A dashed line indicates the point where unliganded, folded MBP is as stable as the unfolded state. Figure adapted from Ref. (40); Copyright (2003) National Academy of Sciences, USA.

analysis of the energetics of domain orientation (40). Both mutational approaches, however, highlight the importance of the balancing interface in stabilizing the open conformation. Indeed, solvent exposure of the interface to the degree displayed by closed-liganded MBP would render an unstable ligand-free structure with a population of approximately 0.001%, as suggested by extrapolation of the experimentally determined closure angle-dependent energy profile (Figure 3), using $\Delta G^{Free}_{Open\rightarrow Closed}$=212·cal/mol/deg×35°=-*RT* ln([*Closed*]/[*Open*]), where *R* is the gas constant, *T*=310 K, and angular brackets indicate the equilibrium concentration of the corresponding conformation. Although extrapolation from small angles (i.e., large interdomain separation) neglects interdomain interactions likely to occur in a putative fully closed, unliganded conformation, they are expected to be unfavorable owing to electrostatic repulsion (41) and lack of surface complementarity to support bridging hydrogen-bonded water molecules (40). The latter are observed replacing the ligand in the closed-unliganded crystal structures of GGBP (15) and ChoX (16), and are suspected to be a significant stabilization factor. These observations reinforce the concept of an unstable closed-unliganded MBP conformation, which has implications with regard to the ligand binding mechanism.

Binding mechanism: population shift vs. induced fit

Two different classic models exist for the ligand binding process in PBPs. The population shift or conformational selection mechanism assumes a PBP spontaneously alternates between an open and a closed conformation, the relative population of which is affected by the ligand: under ligand-free conditions the open form predominates, whereas the introduction of ligand favors or 'selects' the closed conformation thus shifting the equilibrium (42, 43). By contrast, the induced fit model assumes in absence of ligand the closed conformation is inaccessible; consequently, the PBP remains open until interaction with the ligand triggers interdomain closure in a similar manner an insect triggers the closure of a Venus flytrap (2, 44). It is noteworthy that because the closed conformation precludes access to the binding site (Figure 1B), both binding mechanisms require the open conformation for a successful encounter with the ligand, which possibly involves an initial, preferential interaction with one of the domains, as suggested by open-liganded X-ray structures (17–20).

The population shift mechanism is notably supported by the existence of closed-unliganded X-ray structures for GGBP (15) and ChoX (16) [arabinose-binding protein, ABP, has also been mentioned in this select group although no structural details have been provided (3, 45)], the assumption being that such conformations, highly similar to their closed-liganded counterparts, exist in solution and were captured during crystallization. X-ray structures of lysine/arginine/ornithine-binding protein (LAOBP) from *Salmonella typhimurium* also suggest a 'free hinge' model as no obvious trigger mechanism for domain closure is observed: (i) there are neither direct nor indirect (via water molecules) hydrogen bond interactions between the substrate and the hinge in the closed, lysine-loaded structure, and (ii) comparison with the open-unliganded form shows neither water molecule displacement nor side chain movements that can account for the backbone conformational change (43). Interestingly enough, conformation-specific monoclonal antibodies have been found to trap histidine-binding protein (HisJ), also from *S. typhimurium*, in a closed-unliganded conformation in solution (46); HisJ not only shares 70% sequence identity with

the above-mentioned LAOBP molecule but also the same membrane-associated component of the importer.

Structural evidence for the induced fit model of binding stems from the careful study of crystallographic structures, which suggests possible triggering mechanisms for interdomain closure, such as hydrogen bond interactions between the ligand and the hinge, which can be direct [e.g., maltose-Glu111 in MBP (45)] or indirect via network(s) [e.g., Gln-Thr70-Gln183 and Gln-Asp157-Tyr185 in GlnBP (47)]. From a functional perspective, induced fit seems advantageous given that the interaction of the closed conformation itself – and not the substrate – with the transmembrane domains of the importer serves as a translocation signal responsible for eliciting ATPase activity. By contrast, a population shift mechanism implies a small proportion of closed-unliganded conformers capable of unproductive ATP hydrolysis, indeed a 'faulty switch' behavior.

An interesting alternative to the two classic binding models, as described above, has been afforded by paramagnetic NMR. The enhancement of the magnetic relaxation of a nucleus (e.g., that of a peptide backbone H^N) by a paramagnetic label chemically attached to the protein (e.g., nitroxide group) is proportional to r^{-6}, r being the distance between them. This known distance-dependence of the paramagnetic relaxation enhancement (PRE) can be exploited to determine the interdomain arrangement of a PBP in solution, following a rigid-body-domain approach similar to that implemented with RDCs (see above) (48). In contrast to RDCs, however, PREs are additionally sensitive to the existence of lowly populated conformations [for a recent review, see Ref. (49)]. Indeed, owing to the r^{-6} scaling, a particular site in a protein in fast exchange between a major and a minor conformation experiences a population-weighted average PRE which has a significant contribution from the minor species as long as the distance between the site and the spin label is considerably shorter than that in the major species. This situation, schematized in Figure 4, in the context of a minor, closed-unliganded PBP conformer in fast equilibrium with the major, open form, allows the structure determination of the minor species. The strategy was demonstrated with MBP (41) where, in absence of ligand, a minor, closed conformation (approx. 5% population) was detected in coexistence with a major, open one (approx. 95% population), interconverting with a time scale estimated in the 20-μs to 20-ns range. The PRE data were consistent with the major species assuming the open conformation given by the X-ray structure, and the minor species adopting a semi-closed conformation with 33° interdomain closure, in contrast to the 35° of fully closed, liganded MBP. Furthermore, the minor conformer deviates from the common 'closure path' followed by wild-type MBP and several hinge mutants (40) (see previous section), as the domains additionally experience an 18° twist and a 6-Å translation that move the C-domain out of the binding pocket thus avoiding unfavorable electrostatic interactions. Figure 5 compares the minor conformation with that of closed-liganded MBP; the fact that they differ is consistent with an RDC-based NMR study that suggests the latter is unstable (approx. 0.001% population) in absence of

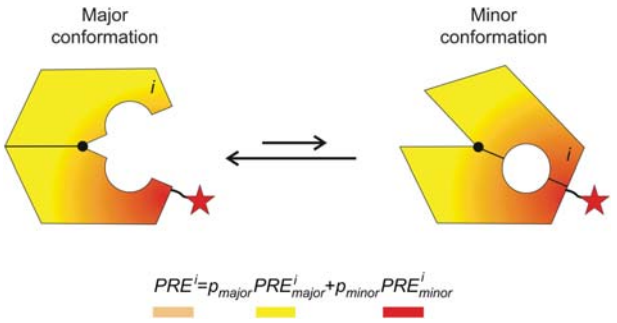

Figure 4 Paramagnetic NMR strategy for structure determination of a minor closed-unliganded PBP conformation in equilibrium with a major open one. A red star represents a spin label, chemically connected to the 'lip' of one domain. The induced distance-dependent paramagnetic relaxation enhancement (PRE) on the protein is graphically indicated via a color gradient, red being the strongest and yellow the weakest. PRE^i, the measured PRE on site i, located in the domain that does not contain the label, considerably reflects that from the minor conformation (PRE^i_{minor}) despite the low population of the latter (p_{minor}). Symbols labeled '*major*' refer to the major conformation (with population $p_{major} \gg p_{minor}$) and are analogous to those associated with the minor species. Although a balancing interface such as that in MBP is implied, it might not apply to all PBPs (14).

ligand owing to, at least in part, exposure of non-polar surface at the balancing interface (40) (Figure 3). Presumably, the twist and translation motion in the approximately 5% populated semi-closed conformer is able to mitigate such exposure and/or counteract it with favorable interactions at the domain-domain interface.

A binding mechanism alternative to those classically proposed is suggested by the structure of the minor, semi-closed conformation of MBP, which displays a partially occluded binding pocket, with a fully exposed C-domain (41). The latter interacts almost exclusively with the ligand in all open-liganded X-ray structures of MBP, which involve maltose

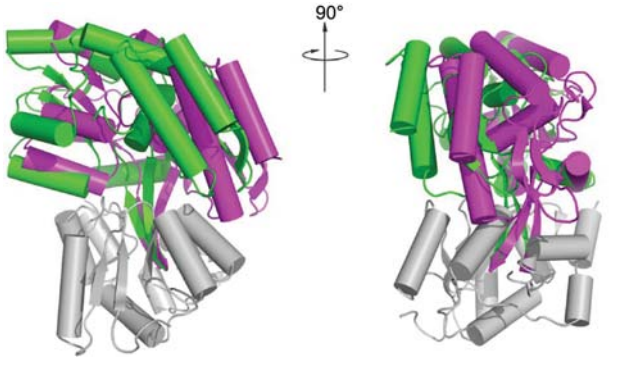

Figure 5 Conformational differences between crystallographic closed-liganded MBP (PDB ID 3MBP; magenta) and the solution, minor, semi-closed-unliganded species (PDB ID 2V93; green). Both structures are superimposed via the N-domain, shown only for the closed-liganded model (gray).

(19), maltotriitol (18), maltotetraitol (18, 19), and the β-cyclodextrin exception that shares this feature only partially as it additionally makes loose contacts with the N-domain (20). In this light, the minor MBP species could act as a binding intermediate that facilitates the transition to the closed-liganded form, a conformational change triggered by ligand-C-domain interactions (41). Such an induced fit mechanism, however, is different from the classic one that takes the open conformation as the starting point; the possibility that both these binding modes are active in MBP cannot be excluded.

The hinge of a PBP balances two competing forces: (i) the tendency to freely allow interdomain movement, an essential feature to achieve the closed-liganded conformation that initiates the ATP-driven import of the substrate, and (ii) the need to discourage such closed conformation in absence of substrate to avoid unfruitful ATP hydrolysis. The above-described minor species of MBP could represent a harmless expression of hinge flexibility that results in a closed conformation different enough from the liganded one, therefore unable to promote significant ATPase activity. Indeed, the minor conformer could explain the ability of unliganded MBP to weakly stimulate ATP hydrolysis (50); such stimulation would presumably be stronger if the minor species had the liganded conformation. Recent findings, however, intriguingly implicate the open conformation of MBP in the substrate-free ATPase levels (51).

In contrast to MBP, a similar paramagnetic NMR study (Figure 4) recently conducted with GlnBP found no evidence of a minor, closed conformation as the open-unliganded X-ray structure was able to appropriately account for the PRE data (30). Such study suggests a different solution to the aforementioned hinge balancing act: a sufficiently rigid hinge to remain open until substrate-mediated closure, i.e., the classic induced fit model. Such rigidity could stem from the strong hydrogen bond interactions between the hinge strands of GlnBP, rarely observed in other PBPs (47). Figure 6 depicts the hinge hydrogen bond connectivity for GlnBP and the PBPs with known closed-unliganded structures. It is noteworthy that whereas GlnBP binds L-glutamine in a highly specific manner, MBP binds a series of maltooligosaccharide substrates of up to seven α(1–4)-linked glucose units. This promiscuity of MBP is shared by GGBP (binds D-glucose and D-galactose), ChoX (choline and acetylcholine) and ABP (L-arabinose, D-galactose, and D-fucose), all involved in closed-unliganded crystal forms (3, 15, 16), and HisJ (L-histidine, L-arginine, and L-lysine) and LAOBP (L-lysine, L-arginine, and L-ornithine), suggested to have closed-unliganded conformations in solution (43, 46). Indeed, an interesting hypothesis is that binding a single substrate could allow a PBP to approach a 'pure switch behavior': a hinge that closes only in presence of the ligand to signal the start of the transmembrane response. By contrast, the need to accommodate several substrates could require a more permissive hinge, the evolutionary advantage of this versatility possibly outweighing unproductive signaling caused by a small population of closed-unliganded conformer. [Note that although a closed-unliganded conformation of RBP – which binds D-ribose only – has been recently suggested by solution NMR data (23), the latter probably reflects residual endogenous ribose as protein purification omitted the denaturation step used elsewhere for this (21) and other PBPs, e.g., Refs. (30, 41), to ensure complete substrate release.]

Interaction with integral membrane proteins of the importer

Whereas PBPs have the important function of recruiting nutrients, the membrane-associated components of ABC importers are responsible for the actual transport. The architecture of such membrane components comprises a conserved core structure of two transmembrane domains (TMDs) and two ATP-binding cassettes (ABCs; also known as nucleotide-binding domains, NBDs) associated to the cytosolic side. The interaction of a closed-liganded PBP with its TMD partners causes ATP hydrolysis (50, 52) and translocation of the substrate across the membrane to the cytoplasm. Although the conformational transitions of PBPs upon substrate binding are well characterized, little is known about the mechanism through which the ligand-bound PBP stimulates ATPase activity.

Based on the eight crystal structures involving intact membrane-associated complexes of ABC transporters solved to date [that in Ref. (53), the rest reviewed in Ref. (13)], each TMD typically contains two modules (Figure 7): (i) a membrane-spanning region where a substrate binding site and the translocation pathway are located, and (ii) an intracytoplasmic loop (ICL) responsible for the association with the ABC. Thus, ICLs are believed to be the region through which the conformational transition following ATP hydrolysis triggers substrate translocation. The membrane-spanning region of a TMD usually consists of six α-helices, although systems with fewer or more helices exist, which could correlate with the different nature of the transported substrates.

X-ray crystallography has additionally been able to provide snapshots of the main conformations at various stages of the transport cycle. In the resting state, the ABC importer adopts an inward-facing conformation (Figure 8A), where the translocation pathway is closed to the periplasm and open to the cytoplasm. In this configuration the ABCs are loosely associated with each other, and the ATP binding pockets are empty. The ligand-bound PBP in the closed conformation docks onto the periplasmic TMD surface, which leads to a rearrangement of the TMDs that is allosterically transmitted (via the ICLs) to the ABCs, which bind ATP and dimerize more tightly. This event, commonly considered as the power stroke for the transport, is associated with the TMDs assuming an outward-facing conformation that allows the opening of the PBP and substrate access to the transmembrane binding site (Figures 7 and 8B). The final step of the transport is represented by ATP hydrolysis and phosphate release that cause the relaxation of the ABC dimer, which in turn opens the cytoplasmic face of the TMDs allowing substrate release into the cytoplasm, and the restart of the cycle.

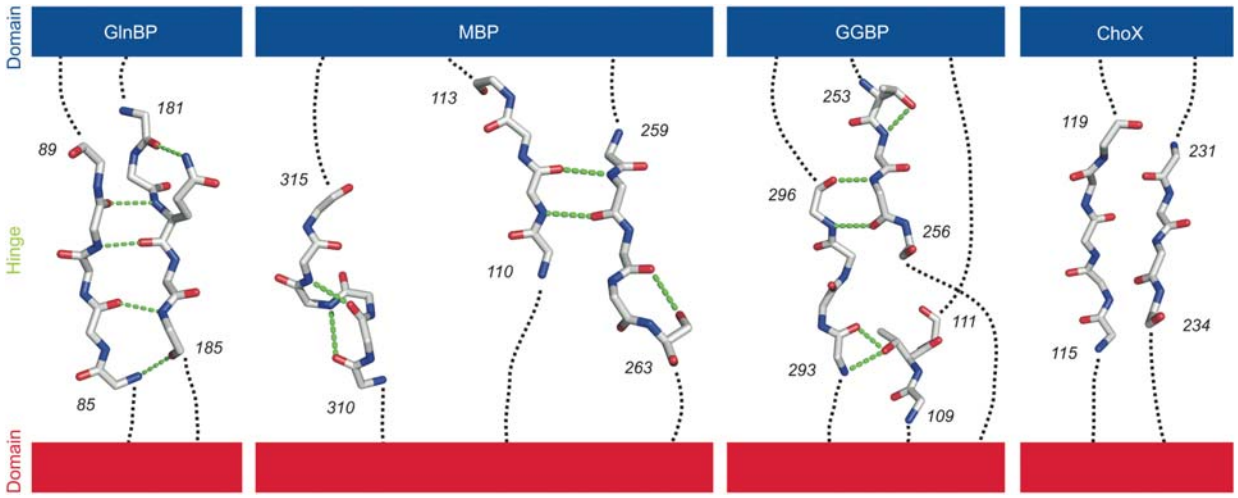

Figure 6 Hydrogen bond connectivity within hinge segments of open-unliganded crystal forms of GlnBP (PDB ID 1GGG), MBP (PDB ID 1OMP), GGBP (PDB ID 2FW0), and ChoX (PDB ID 3HCQ). Residue numbers at the end of each segment are indicated. Green, dashed lines denote hydrogen bonds. Side chains involved in hydrogen bonding are shown, as well as the complete polypeptide backbone (only heavy atoms included: C, gray; O, red; N, blue). Backbone covalent connections to the PBP domains are indicated by black, dotted lines. The domains are represented by red and blue rectangles (e.g., the N- and C-domains of MBP are denoted red and blue, respectively, as in Figure 1). Figure adapted from Ref. (30).

Atomic level knowledge on the PBP-TMD interaction has been afforded by the crystal structures of intact importers (54, 55). In the case of the maltose transport system, the TMDs, called MalF and MalG, have periplasmic loop regions involved in functional contacts with MBP. In the crystal structure (55) (Figure 7), the periplasmic loop P3 of MalG is located close to the substrate-binding site of MBP, and has been proposed to help release the substrate. The periplasmic loop P2 of MalF, by contrast, extends approximately 30 Å towards the periplasm where it binds on top of the N-domain of MBP (Figure 7). Although the P2 loop displays a well-defined two-domain fold when bound to MBP, crystallographic studies on the MBP-free importer have been unable to determine its structure (56).

To investigate whether in absence of MBP the P2 loop is folded in solution, NMR studies have been performed on the loop isolated from MalF (57). It was found that the individual domains adopt a well-defined structure in solution, very similar to that in the crystal (Figure 7), although with a different average interdomain orientation. The measured rotational correlation time of approximately 8.4 ns is typical of small globular proteins of approximately 15 kDa, in contrast to the 18 kDa of the P2 loop, a difference that can be explained by the two domains independently tumbling in solution. This finding could be the reason why it was difficult to interpret the crystal density map of the loop in the MBP-free importer (56), even if the individual domains were able to adopt a well-defined fold.

Because in the X-ray structure of the MBP-bound importer the P2 loop does not have stabilizing interactions with other parts of the TMDs, and binds only to MBP (Figure 7), the isolated loop was considered a good candidate to study the interaction of MBP with the rest of the transporter (57). The

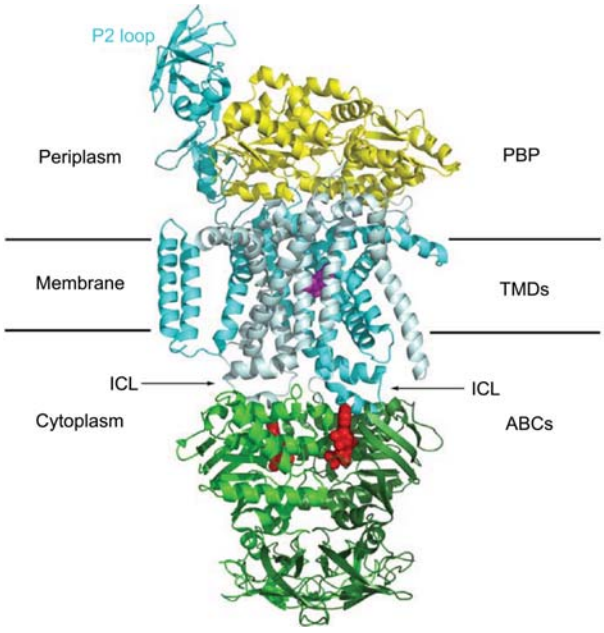

Figure 7 Crystal structure of the complete maltose importer (PDB ID 2R6G), an example of the ABC transporter superfamily. Protein backbone trace is shown, with the PBP (MBP) in yellow, and the two TMDs (MalF and MalG) and ABCs in blue and green, respectively, with different tones for each monomer. Atoms of a maltose substrate molecule are shown as magenta spheres occupying the transmembrane binding site. Atoms of two ATP molecules are displayed as red spheres at their corresponding ABC sites. The position of the membrane (horizontal lines) was chosen to correspond to the predicted buried residues of the TMDs.

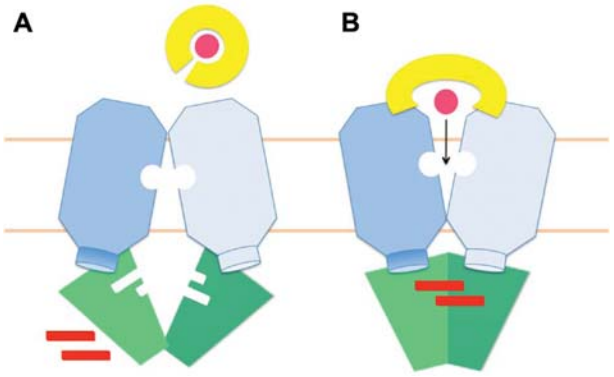

Figure 8 Schematic representation of inward-facing (A) and outward-facing (B) conformations of ABC importers. The color codes of the different subunits are indicated in the caption to Figure 7; the latter corresponds to an outward-facing configuration (B).

P2 loop was found to bind MBP both in the presence and in the absence of maltose, as confirmed by isothermal titration calorimetry, and this independence on substrate presence is clear if one observes that the loop interacts only with the N-domain of MBP. In the solution, MBP-bound form, the structure of domain 1 of the P2 loop remains unperturbed when compared to its MBP-free version, whereas the relative orientation of the two domains changes. This orientation change to accommodate MBP leads to a conformational change in domain 2 that shows significant differences, mainly on the surface, relative to the free form and, consequently, also relative to the X-ray MBP-bound form, suspected to suffer from crystal contacts (57).

The central role of exceptionally long periplasmic loops, such as MalF-P2, characteristic of enterobacteria, raises the question of how the majority of importers, which lack extended periplasmic regions, signal the presence of substrate to the membrane-associated components of the importer.

The other side of the membrane

The interaction of a substrate-bound PBP with its associated TMDs serves as a signal that ultimately reaches the ABCs across the plasma membrane. ABCs are L-shaped peripheral membrane proteins with two lobes and three subdomains (14) (Figure 7). Lobe I includes the RecA-like subdomain, comprising the Walker A and B motifs, and the β-sheet subdomain. Lobe II is an α-helical subdomain containing the LSGGQ signature sequence that is unique to the ABC transporters and defines the ABC superfamily.

ABCs work as dimers arranged in a head-to-tail conformation and bind two ATP molecules in a sandwich-like manner so that the nucleotides are embedded in the binding interface. In particular, these binding sites are represented by Walker A and B motifs from one monomer and signature sequence from the other monomer (58, 59). This conformation has been observed by X-ray crystallography in both isolated ABCs (59–66) and complete transport systems (67–71). ABCs share a high degree of sequence similarity and identity, being the most conserved components of the transport system. Many regions are highly conserved, such as Walker A and B motifs, and the signature sequence, suggesting a common mode of coupling ATP hydrolysis to TMD movement (12). Therefore, the study of ABCs even from systems that do not rely on PBPs can help provide insights on PBP-dependent import.

Because solution studies of TMDs, and integral membrane proteins in general, are challenging, most of the NMR work on the membrane-associated components of ABC systems has been conducted on the ABC cassettes that are easier to solubilize. Such investigations notably involve the cystic fibrosis transmembrane conductance regulator (CFTR) and MJ1267 ABC from *Methanococcus jannaschii* [for additional work, see the recent review in Ref. (72)].

CFTR is a mammalian ABC-based ion channel responsible for the transport of thiocyanate and chloride across epithelial cell membranes. Although encoded as a single chain, CFTR shares a common domain organization with bacterial ABC importers, except for the existence of a characteristic accessory domain, the hydrophilic regulatory domain R, which contains various serines as phosphorylation sites. Cystic fibrosis is caused by point mutations, the most common being the deletion of F508 (ΔF508) within the first ABC, referred to as NBD1. This deletion causes the protein to be retained by the endoplasmic reticulum (ER) and be degraded.

The effect of the F508 deletion on the structure of peptides around the mutation region have been investigated by NMR (73), revealing that the wild-type peptide adopts an α-helical structure with the F508 residue lying within the helix. By contrast, a peptide corresponding to the deletion mutant ΔF508 shows a lesser propensity of forming well-defined secondary structure in solution. Such structural differences in ΔF508 could prevent CFTR from undergoing the conformational transition necessary to be released by the ER (74), thus avoiding degradation caused by misfolding.

The CFTR channel gating properties are controlled by both ATP hydrolysis (at the ABCs) and phosphorylation (at the R-domain). The R-domain has been postulated to have phosphorylation-dependent interactions with the ABCs, and its properties have been successfully investigated by NMR (75), affording a dynamic picture of its possible conformations in solution. NMR data on the R-domain suggest it is mainly disordered, with a certain propensity of some fragments towards α-helical structure. In the presence of NBD1 many regions of the R-domain remain unstructured with different mobility, whereas the fragments with helical propensity are transiently stabilized in an α-helix. The interactions between R-domain and NBD1 are weakened by phosphorylation, where the entire R-domain becomes disordered, and the overall mobility increases. Because in crystals the α-helical region of R-domain binds NBD1 at the putative dimer interface between NBD1 and NBD2 – the other ABC – unphosphorylated R-domain is believed to inhibit ABC dimerization, whereas its unfolding and subsequent unbinding upon phosphorylation promotes ABC association and ATP cycling.

Further NMR work has shed light on the mechanism underlying regulation of CFTR and its dysfunction in the disease (76). Specifically, the study probed the interactions of NBD1 with coupling helix 1 of the ICL, responsible for coupling ATP hydrolysis to transport, in addition to the role of the R-domain in modulating such interactions. It was found that whereas phosphorylation promotes the interaction of NBD1 with coupling helix 1, it weakens the fluctuating interactions between NBD1 and the R-domain. The latter is consistent with previous NMR work (75) (discussed above) and could explain increased ATPase activity observed for the phosphorylated protein (76). In the ΔF508 mutant, however, the interactions between NBD1 and the R-domain are not disrupted upon phosphorylation, thus inhibiting the binding with coupling helix 1. These structural and dynamic differences are believed to be responsible for the dysfunction of the disease-causing deletion.

Solution NMR has been applied to the study of MJ1267 to further characterize the conformational and dynamic properties of ABCs, and explore the coupling of these properties to the ATP hydrolysis reaction cycle (77). MJ1267 from *Methanococcus jannaschii* is the single-chain ABC of a transporter responsible for the uptake of leucine, isoleucine, and valine. MJ1267 presents in the α-helical subdomain a region termed LivG insert, which, by homology with other ABCs, has been localized in a region responsible for the communication with the TMD (77). ADP-Mg binding to MJ1267 strongly affected several NMR spectral signals, including those of the Walker A and B motifs, and LivG insert. This indicates major conformational changes in these areas, which are allosteric in the case of LivG insert as it is located 30 Å away from the nucleotide-binding site. The fact that NMR dynamics experiments indicate LivG insert is mobile on the μs–ms time scale, in both the apo and ADP-Mg-bound states, thus suggests that ADP-Mg allosterically changes the distribution and/or nature of the dynamically visited conformations. Such changes could be important for energy coupling to TMD conformational transitions and thus to the transport. Concomitantly with nucleotide binding, further NMR dynamics analysis on the μs–ms time scale revealed that although several regions in contact with ADP-Mg in the known crystal structure remain flexible, others such as the Walker A and the aromatic residue responsible for adenosine stacking (F17) experience a restriction in their mobility. These dynamic changes are consistent with a population shift model of binding, discussed in a previous section in the context of PBPs.

Although many structures of ABCs have been solved both as monomers and dimers, the mechanism through which ATP hydrolysis provides energy for transport is not completely clear. Considering the high sequence identity among ABCs from different transport systems, it is realistic to think that a common mechanism might exist. A complicating factor, however, is the existence of both homodimer ABCs (e.g., MJ1267) and heterodimer ABCs (e.g., CFTR). The fact that in the latter class the single monomers show distinct ATP affinity and hydrolyzing capabilities leads to question if the two classes of ABCs behave in the same manner. For instance, it would be interesting to verify if homodimers hydrolyze ATP in a concerted manner whereas heterodimers use the so-called alternating catalytic sites model (78).

Conclusions

The atomic level study of PBPs and related transport proteins highlights the synergy between the two main techniques available to structural biology: while X-ray crystallography has been invaluable in providing static molecular pictures, solution NMR has taken advantage of such information, notably, to enrich our understanding on the dynamic properties of such systems. Thus, for instance, studies on MJ1267 ABC, at the cytoplasmic end of the transport process, indicate that nucleotide binding allosterically affects the dynamics of the region in contact with the TMD, a possible mechanism to communicate the occupancy state of the ATP binding site to the rest of the system (77). On the periplasmic end, NMR has helped tackle long-standing questions regarding PBP open-closed transitions and ligand binding. Such studies suggest that, as far as MBP (40, 41) and GlnBP (30) are concerned, the closed conformations are inherently unstable and require substrate-PBP interactions (encapsulated in $\Delta G^{Closed}_{Binding}$; see Figure 2 for this and the following free-energy expressions) to overcome the significant energetic cost of the open → closed deformation, $\Delta G^{Free}_{Open \rightarrow Closed}$. The handling of several different substrates by a single PBP could represent an efficiency gain. However, such versatility could require lowering $\Delta G^{Free}_{Open \rightarrow Closed}$ (i.e., favoring a closed-unliganded state) to accommodate the substrate that contributes less towards the stabilization of the closed conformation, and achieve the characteristic tight binding [small $\Delta G^{App}_{Binding}$; see Eq. (1)], probably needed for efficient substrate uptake against an uphill concentration gradient. This could explain the ability of MBP to reach a semi-closed-unliganded conformation in solution (41). By contrast, when only a single substrate has to be bound, the closed form might be as unstable as the favorable interactions with the substrate allow it to be while still achieving a high binding affinity. The advantage of this situation is the discouragement of a closed-unliganded conformation that could falsely signal substrate presence to the rest of the importer, thus eliciting ATP hydrolysis. At least to a certain extent, this might be the case of GlnBP, and explain the lack of support for a ligand-free closed conformation in solution for this system (30).

Acknowledgments

This work was supported by the NHLBI and CIT Intramural Research Programs of the NIH to N.T. and G.A.B., respectively.

References

1. Holland IB, Cole SPC, Kuchler K, Higgins CF, editors. ABC proteins: from bacteria to man, 1st ed., Amsterdam/Boston, MA: Academic Press, 2003.

2. Quiocho FA. Atomic structures of periplasmic binding-proteins and the high-affinity active-transport systems in bacteria. Philos Trans R Soc Lond B 1990; 326: 341–52.
3. Quiocho FA. Atomic structures and function of periplasmic receptors for active transport and chemotaxis. Curr Opin Struct Biol 1991; 1: 922–33.
4. Tam R, Saier MH. Structural, functional, and evolutionary relationships among extracellular solute-binding receptors of bacteria. Microbiol Rev 1993; 57: 320–46.
5. Quiocho FA, Ledvina PS. Atomic structure and specificity of bacterial periplasmic receptors for active transport and chemotaxis: variation of common themes. Mol Microbiol 1996; 20: 17–25.
6. Felder CB, Graul RC, Lee AY, Merkle HP, Sadee W. The Venus flytrap of periplasmic binding proteins: an ancient protein module present in multiple drug receptors. AAPS PharmSci 1999; 1: E2.
7. Wilkinson AJ, Verschueren KHG. Crystal structures of periplasmic solute-binding proteins in ABC transport complexes illuminate their function. In: Holland IB, Cole SPC, Kuchler K, Higgins CF, editors. ABC proteins: from bacteria to man, 1st ed., Amsterdam/Boston, MA: Academic Press, 2003: 187–207.
8. Hollenstein K, Dawson RJP, Locher KP. Structure and mechanism of ABC transporter proteins. Curr Opin Struct Biol 2007; 17: 412–8.
9. Jones PM, George AM. The ABC transporter structure and mechanism: perspectives on recent research. Cell Mol Life Sci 2004; 61: 682–99.
10. Jones PM, O'Mara ML, George AM. ABC transporters: a riddle wrapped in a mystery inside an enigma. Trends Biochem Sci 2009; 34: 520–31.
11. Kos V, Ford RC. The ATP-binding cassette family: a structural perspective. Cell Mol Life Sci 2009; 66: 3111–26.
12. Oldham ML, Davidson AL, Chen J. Structural insights into ABC transporter mechanism. Curr Opin Struct Biol 2008; 18: 726–33.
13. Rees DC, Johnson E, Lewinson O. ABC transporters: the power to change. Nat Rev Mol Cell Biol 2009; 10: 218–27.
14. Davidson AL, Dassa E, Orelle C, Chen J. Structure, function, and evolution of bacterial ATP-binding cassette systems. Microbiol Mol Biol Rev 2008; 72: 317–64.
15. Flocco MM, Mowbray SL. The 1.9 Angstrom X-ray structure of a closed unliganded form of the periplasmic glucose/galactose receptor from Salmonella typhimurium. J Biol Chem 1994; 269: 8931–6.
16. Oswald C, Smits SHJ, Hoing M, Sohn-Bosser L, Dupont L, Le Rudulier D, Schmitt L, Bremer E. Crystal structures of the choline/acetylcholine substrate-binding protein ChoX from Sinorhizobium meliloti in the liganded and unliganded-closed states. J Biol Chem 2008; 283: 32848–59.
17. Sack JS, Saper MA, Quiocho FA. Periplasmic binding-protein structure and function – refined X-ray structures of the leucine/isoleucine/valine-binding protein and its complex with leucine. J Mol Biol 1989; 206: 171–91.
18. Duan XQ, Hall JA, Nikaido H, Quiocho FA. Crystal structures of the maltodextrin/maltose-binding protein complexed with reduced oligosaccharides: flexibility of tertiary structure and ligand binding. J Mol Biol 2001; 306: 1115–26.
19. Duan XQ, Quiocho FA. Structural evidence for a dominant role of nonpolar interactions in the binding of a transport/chemosensory receptor to its highly polar ligands. Biochemistry 2002; 41: 706–12.
20. Sharff AJ, Rodseth LE, Quiocho FA. Refined 1.8-Angstrom structure reveals the mode of binding of beta-cyclodextrin to the maltodextrin binding-protein. Biochemistry 1993; 32: 10553–9.
21. Björkman AJ, Mowbray SL. Multiple open forms of ribose-binding protein trace the path of its conformational change. J Mol Biol 1998; 279: 651–64.
22. Magnusson U, Chaudhuri BN, Ko J, Park C, Jones TA, Mowbray SL. Hinge-bending motion of D-allose-binding protein from Escherichia coli – three open conformations. J Biol Chem 2002; 277: 14077–84.
23. Schreier B, Stumpp C, Wiesner S, Höcker B. Computational design of ligand binding is not a solved problem. Proc Natl Acad Sci USA 2009; 106: 18491–6.
24. Trakhanov S, Vyas NK, Luecke H, Kristensen DM, Ma JP, Quiocho FA. Ligand-free and -bound structures of the binding protein (LivJ) of the Escherichia coli ABC leucine/isoleucine/valine transport system: trajectory and dynamics of the interdomain rotation and ligand specificity. Biochemistry 2005; 44: 6597–608.
25. Oswald C, Smits SH, Hoing M, Bremer E, Schmitt L. Structural analysis of the choline-binding protein ChoX in a semi-closed and ligand-free conformation. Biol Chem 2009; 390: 1163–70.
26. Magnusson U, Salopek-Sondi B, Luck LA, Mowbray SL. X-ray structures of the leucine-binding protein illustrate conformational changes and the basis of ligand specificity. J Biol Chem 2004; 279: 8747–52.
27. Sack JS, Trakhanov SD, Tsigannik IH, Quiocho FA. Structure of the L-leucine-binding protein refined at 2.4 Å resolution and comparison with the Leu/Ile/Val-binding protein-structure. J Mol Biol 1989; 206: 193–207.
28. Borrok MJ, Kiessling LL, Forest KT. Conformational changes of glucose/galactose-binding protein illuminated by open, unliganded, and ultra-high-resolution ligand-bound structures. Protein Sci 2007; 16: 1032–41.
29. Evenäs J, Tugarinov V, Skrynnikov NR, Goto NK, Muhandiram R, Kay LE. Ligand-induced structural changes to maltodextrin-binding protein as studied by solution NMR spectroscopy. J Mol Biol 2001; 309: 961–74.
30. Bermejo GA, Strub MP, Ho C, Tjandra N. Ligand-free open-closed transitions of periplasmic binding proteins: the case of glutamine-binding protein. Biochemistry 2010; 49: 1893–902.
31. Telmer PG, Shilton BH. Insights into the conformational equilibria of maltose-binding protein by analysis of high affinity mutants. J Biol Chem 2003; 278: 34555–67.
32. Mueller GA, Choy WY, Yang DW, Forman-Kay JD, Venters RA, Kay LE. Global folds of proteins with low densities of NOEs using residual dipolar couplings: application to the 370-residue maltodextrin-binding protein. J Mol Biol 2000; 300: 197–212.
33. Bax A, Kontaxis G, Tjandra N. Dipolar couplings in macromolecular structure determination. Method Enzymol 2001; 339: 127–74.
34. Skrynnikov NR, Goto NK, Yang DW, Choy WY, Tolman JR, Mueller GA, Kay LE. Orienting domains in proteins using dipolar couplings measured by liquid-state NMR: differences in solution and crystal forms of maltodextrin binding protein loaded with β-cyclodextrin. J Mol Biol 2000; 295: 1265–73.
35. Hwang PM, Skrynnikov NR, Kay LE. Domain orientation in β-cyclodextrin-loaded maltose binding protein: diffusion anisotropy measurements confirm the results of a dipolar coupling study. J Biomol NMR 2001; 20: 83–8.
36. Kay LE. Nuclear magnetic resonance methods for high molecular weight proteins: a study involving a complex of maltose binding protein and β-cyclodextrin. Method Enzymol 2001; 339: 174–203.

37. Dwyer MA, Hellinga HW. Periplasmic binding proteins: a versatile superfamily for protein engineering. Curr Opin Struct Biol 2004; 14: 495–504.
38. Medintz IL, Deschamps JR. Maltose-binding protein: a versatile platform for prototyping biosensing. Curr Opin Biotechnol 2006; 17: 17–27.
39. Marvin JS, Hellinga HW. Manipulation of ligand binding affinity by exploitation of conformational coupling. Nature Struct Biol 2001; 8: 795–8.
40. Millet O, Hudson RP, Kay LE. The energetic cost of domain reorientation in maltose-binding protein as studied by NMR and fluorescence spectroscopy. Proc Natl Acad Sci USA 2003; 100: 12700–5.
41. Tang C, Schwieters CD, Clore GM. Open-to-closed transition in apo maltose-binding protein observed by paramagnetic NMR. Nature 2007; 449: 1078–82.
42. Walmsley AR, Shaw JG, Kelly DJ. Perturbation of the equilibrium between open and closed conformations of the periplasmic C4-dicarboxylate binding-protein from Rhodobacter capsulatus. Biochemistry 1992; 31: 11175–81.
43. Oh BH, Pandit J, Kang CH, Nikaido K, Gokcen S, Ames GFL, Kim SH. 3-Dimensional structures of the periplasmic lysine/arginine/ornithine-binding protein with and without a ligand. J Biol Chem 1993; 268: 11348–55.
44. Mao B, Pear MR, McCammon JA, Quiocho FA. Hinge-bending in L-arabinose-binding protein. The ''Venus's-flytrap'' model. J Biol Chem 1982; 257: 1131–3.
45. Sharff AJ, Rodseth LE, Spurlino JC, Quiocho FA. Crystallographic evidence of a large ligand-induced hinge-twist motion between the 2 domains of the maltodextrin binding-protein involved in active-transport and chemotaxis. Biochemistry 1992; 31: 10657–63.
46. Wolf A, Shaw EW, Nikaido K, Ames GFL. The histidine-binding protein undergoes conformational-changes in the absence of ligand as analyzed with conformation-specific monoclonal antibodies. J Biol Chem 1994; 269: 23051–8.
47. Sun YJ, Rose J, Wang BC, Hsiao CD. The structure of glutamine-binding protein complexed with glutamine at 1.94 angstrom resolution: comparisons with other amino acid binding proteins. J Mol Biol 1998; 278: 219–29.
48. Bermejo GA, Strub MP, Ho C, Tjandra N. Determination of the solution bound conformation of an amino acid binding protein by NMR paramagnetic relaxation enhancement: use of a single flexible paramagnetic probe with improved estimation of its sampling space. J Am Chem Soc 2009; 131: 9532–7.
49. Clore GM, Iwahara J. Theory, practice, and applications of paramagnetic relaxation enhancement for the characterization of transient low-population states of biological macromolecules and their complexes. Chem Rev 2009; 109: 4108–39.
50. Davidson AL, Shuman HA, Nikaido H. Mechanism of maltose transport in Escherichia coli – transmembrane signaling by periplasmic binding-proteins. Proc Natl Acad Sci USA 1992; 89: 2360–4.
51. Gould AD, Telmer PG, Shilton BH. Stimulation of the maltose transporter ATPase by unliganded maltose binding protein. Biochemistry 2009; 48: 8051–61.
52. Petronilli V, Ames GF. Binding protein-independent histidine permease mutants – uncoupling of ATP hydrolysis from transmembrane signaling. J Biol Chem 1991; 266: 16293–6.
53. Aller SG, Yu J, Ward A, Weng Y, Chittaboina S, Zhuo RP, Harrell PM, Trinh YT, Zhang QH, Urbatsch IL, Chang G. Structure of P-glycoprotein reveals a molecular basis for polyspecific drug binding. Science 2009; 323: 1718–22.
54. Hvorup RN, Goetz BA, Niederer M, Hollenstein K, Perozo E, Locher KP. Asymmetry in the structure of the ABC transporter-binding protein complex BtuCD-BtuF. Science 2007; 317: 1387–90.
55. Oldham ML, Khare D, Quiocho FA, Davidson AL, Chen J. Crystal structure of a catalytic intermediate of the maltose transporter. Nature 2007; 450: 515–21.
56. Khare D, Oldham ML, Orelle C, Davidson AL, Chen J. Alternating access in maltose transporter mediated by rigid-body rotations. Mol Cell 2009; 33: 528–36.
57. Jacso T, Grote M, Daus ML, Schmieder P, Keller S, Schneider E, Reif B. Periplasmic loop P2 of the MalF subunit of the maltose ATP binding cassette transporter is sufficient to bind the maltose binding protein MalE. Biochemistry 2009; 48: 2216–25.
58. Jones PM, George AM. Subunit interactions in ABC transporters: towards a functional architecture. FEMS Microbiol Lett 1999; 179: 187–202.
59. Smith PC, Karpowich N, Millen L, Moody JE, Rosen J, Thomas PJ, Hunt JF. ATP binding to the motor domain from an ABC transporter drives formation of a nucleotide sandwich dimer. Mol Cell 2002; 10: 139–49.
60. Chen J, Lu G, Lin J, Davidson AL, Quiocho FA. A tweezers-like motion of the ATP-binding cassette dimer in an ABC transport cycle. Mol Cell 2003; 12: 651–61.
61. Hopfner KP, Karcher A, Shin DS, Craig L, Arthur LM, Carney JP, Tainer JA. Structural biology of Rad50 ATPase: ATP-driven conformational control in DNA double-strand break repair and the ABC-ATPase superfamily. Cell 2000; 101: 789–800.
62. Hung LW, Wang IX, Nikaido K, Liu PQ, Ames GF, Kim SH. Crystal structure of the ATP-binding subunit of an ABC transporter. Nature 1998; 396: 703–7.
63. Lamers MH, Perrakis A, Enzlin JH, Winterwerp HHK, de Wind N, Sixma TK. The crystal structure of DNA mismatch repair protein MutS binding to a G×T mismatch. Nature 2000; 407: 711–7.
64. Obmolova G, Ban C, Hsieh P, Yang W. Crystal structures of mismatch repair protein MutS and its complex with a substrate DNA. Nature 2000; 407: 703–10.
65. Pakotiprapha D, Inuzuka Y, Bowman BR, Moolenaar GF, Goosen N, Jeruzalmi D, Verdinel GL. Crystal structure of Bacillus stearothermophilus UvrA provides insight into ATP-modulated dimerization, UvrB interaction, and DNA binding. Mol Cell 2008; 29: 122–33.
66. Verdon G, Albers SV, Dijkstra BW, Driessen AJM, Thunnissen AMWH. Crystal structures of the ATPase subunit of the glucose ABC transporter from Sulfolobus solfataricus: nucleotide-free and nucleotide-bound conformations. J Mol Biol 2003; 330: 343–58.
67. Chen J, Sharma S, Quiocho FA, Davidson AL. Trapping the transition state of an ATP-binding cassette transporter: evidence for a concerted mechanism of maltose transport. Proc Natl Acad Sci USA 2001; 98: 1525–30.
68. Janas E, Hofacker M, Chen M, Gompf S, van der Does C, Tampe R. The ATP hydrolysis cycle of the nucleotide-binding domain of the mitochondrial ATP-binding cassette transporter Mdl1p. J Biol Chem 2003; 278: 26862–9.
69. Loo TW, Bartlett MC, Clarke DM. The ''LSGGQ'' motif in each nucleotide-binding domain of human P-glycoprotein is adjacent to the opposing Walker A sequence. J Biol Chem 2002; 277: 41303–6.
70. Moody JE, Millen L, Binns D, Hunt JF, Thomas PJ. Cooperative, ATP-dependent association of the nucleotide binding cassettes during the catalytic cycle of ATP-binding cassette transporters. J Biol Chem 2002; 277: 21111–4.
71. Zaitseva J, Oswald C, Jumpertz T, Jenewein S, Wiedenmann

A, Holland IB, Schmitt L. A structural analysis of asymmetry required for catalytic activity of an ABC-ATPase domain dimer. EMBO J 2006; 25: 3432–43.
72. Hellmich UA, Glaubitz C. NMR and EPR studies of membrane transporters. Biol Chem 2009; 390: 815–34.
73. Massiah MA, Ko YH, Pedersen PL, Mildvan AS. Cystic fibrosis transmembrane conductance regulator: solution structures of peptides based on the Phe508 region, the most common site of disease-causing ΔF508 mutation. Biochemistry 1999; 38: 7453–61.
74. Lukacs GL, Mohamed A, Kartner N, Chang XB, Riordan JR, Grinstein S. Conformational maturation of CFTR but not its mutant counterpart (ΔF508) occurs in the endoplasmic reticulum and requires ATP. EMBO J 1994; 13: 6076–86.
75. Baker JMR, Hudson RP, Kanelis V, Choy WY, Thibodeau PH, Thomas PJ, Forman-Kay JD. CFTR regulatory region interacts with NBD1 predominantly via multiple transient helices. Nature Struct Mol Biol 2007; 14: 738–45.
76. Kanelis V, Hudson RP, Thibodeau PH, Thomas PJ, Forman-Kay JD. NMR evidence for differential phosphorylation-dependent interactions in WT and ΔF508 CFTR. EMBO J 2010; 29: 263–77.
77. Wang CY, Karpowich N, Hunt JF, Rance M, Palmer AG. Dynamics of ATP-binding cassette contribute to allosteric control, nucleotide binding and energy transduction in ABC transporters. J Mol Biol 2004; 342: 525–37.
78. Senior AE, Al-Shawi MK, Urbatsch IL. The catalytic cycle of P-glycoprotein. FEBS Lett 1995; 377: 285–9.